Materials Today Bio 19 (2023) 100558

Contents lists available at ScienceDirect

Materials Today Bio

journal homepage: www.journals.elsevier.com/materials-today-bio

An injectable and self-healing hydrogel with dual physical crosslinking for in-situ bone formation

Tao Yu [a,1], Yunping Hu [b,1], Wenbao He [c,1], Yong Xu [f], Anqi Zhan [f], Kai Chen [b], Mingxiang Liu [b], Xiufeng Xiao [b,*], Xiangyang Xu [a,**], Qian Feng [e,***], Liangfu Jiang [d,****]

[a] Department of Orthopaedics, Ruijin Hospital, Shanghai Jiao Tong University School of Medicine, Shanghai, China
[b] Fujian Provincial Key Laboratory of Advanced Materials Oriented Chemical Engineering, College of Chemistry and Materials Science, Fujian Normal University, Fuzhou, China
[c] Department of Orthopedics, Shanghai Tongji Hospital, School of Medicine, Tongji University, Shanghai, China
[d] Department of Orthopedics (Division of Wound Repair), The Second Affiliated Hospital and Yuying Children's Hospital of Wenzhou Medical University, Wenzhou, China
[e] Key Laboratory of Biorheological Science and Technology, Ministry of Education, College of Bioengineering, Chongqing University, Chongqing, China
[f] Shanghai Key Laboratory of Tissue Engineering, Shanghai Ninth People's Hospital, Shanghai JiaoTong University School of Medicine, Shanghai, China

ARTICLE INFO

Keywords:
Hydrogel
Mechanical properties
Osteogenesis
Physical crosslinking
Self-healing

ABSTRACT

Although hydrogels have been widely studied because of their satisfactory biocompatibility and plasticity, their application is limited in bone tissue engineering (BTE) owing to their inadequate mechanical properties and absence of osteogenic activity. To address this issue, we developed an updated alendronate (ALN)-Ca^{2+}/Mg^{2+}-doped supramolecular (CMS) hydrogel based on our previously developed mechanically resilient "host-guest macromer" (HGM) hydrogel to improve the hydrogel's mechanical properties and osteogenic activity. The CMS hydrogel was prepared by introducing a new physical crosslinking comprising the strong chelation of the comonomer acrylate alendronate (Ac-ALN) and Ca^{2+}/Mg^{2+} in the HGM hydrogel. Compared with the previously developed HGM hydrogel, the upgraded CMS hydrogel presented better mechanical properties because of the additional physical crosslinking, while possessing injectable and self-healing properties like the HGM hydrogel. Moreover, the addition of Ac-ALN and Ca^{2+}/Mg^{2+} also effectively promoted the *in vitro* proliferation, migration, and osteogenic differentiation of bone marrow-derived stem cells. The healing effect of a rat cranial defect further proved that the *in vivo* bone regeneration ability of CMS hydrogel was better than that of HGM hydrogel. The updated CMS hydrogel shows significant potential for BTE application.

1. Introduction

More than two million bone graft surgeries are performed worldwide each year [1]. Bone defects due to various events (such as trauma, tumors, and infections) [2] often require secondary or multiple surgeries because the existing surgical procedures, including autologous or allogeneic bone grafting and bone cement filling, are not applicable for various kinds of bone defects [3]. Consequently, repeated open surgeries considerably increase the medical risks during the treatment process [4]. Thus, there is an urgent need to develop a new modality to effectively repair bone defects.

Bone tissue engineering (BTE), representing the intersecting development of material science and regenerative medicine, is promising as an ideal treatment for bone defects [5]. A considerable number of natural or synthetic biomaterials developed for the utilization of BTE have shown efficacy in repairing bone defects [6]. Among them, thermosensitive hydrogels with in-situ gelation properties are widely studied owing to their ability to transition from a liquid state to a solid gel state at body temperature and subsequent suitability for injection applications [7]. Moreover, because of this property, injectable hydrogels are favored for bone defect repair as they can fill in geometrically complex and irregular spaces using a minimally invasive procedure [8]. Nevertheless, several

* Corresponding author.
** Corresponding author.
*** Corresponding author.
**** Corresponding author.
E-mail addresses: xfxiao@fjnu.edu.cn (X. Xiao), xu664531@163.com (X. Xu), qianfeng@cqu.edu.cn (Q. Feng), jiangliangfu@wmu.edu.cn (L. Jiang).
[1] These authors contributed equal to this work.

https://doi.org/10.1016/j.mtbio.2023.100558
Received 8 September 2022; Received in revised form 18 January 2023; Accepted 19 January 2023
Available online 24 January 2023

hydrogels do not meet the criteria to be used in bone tissue applications because of their inadequate mechanical properties required for load-bearing defects, and without the addition of osteogenic biological factors, the hydrogels loaded with stem cells are inefficient in repairing bone defects [9]. Consequently, an ideal hydrogel for BTE utilization should fulfill two critical requirements: possess an excellent pro-osteogenic capacity and eligible mechanical properties.

In our previous study, we developed a multifunctional "host-guest macromer" (HGM) supramolecular hydrogel system [10]. The crosslinking formation of this HGM hydrogel is based on the weak host-guest interaction between the polymerized acryl β-cyclodextrins (β-CD) and the aromatic groups of the gelatin backbone, which contributes to the properties of mechanical resilience, injectability, bio-adhesion, and cell-infiltration of the HGM hydrogel. All these properties imparted HGM hydrogel with good efficiency for tissue regeneration even without exogenous cell encapsulation. Yet, this hydrogel's mechanical property is still unsatisfactory as it also lacks bioactivity to further accelerate bone regeneration.

Therefore, we have been committed to solving the above two problems and aiming to develop a refined HGM-based hydrogel with an enhanced excellent mechanical property and improved osteogenic bioactivity for BTE. Alendronate (ALN), a United States Food and Drug Administration (FDA) approved drug [11,12], is the first-line clinical drug for the treatment of osteoporosis, which not only inhibits the activity and proliferation of osteoclasts but also has a significant effect on the differentiation of stem cells into osteoblasts [13,14]. ALN promotes mesenchymal stem cell differentiation toward osteogenesis by activating the mitogen-activated protein kinase signaling pathway [15]. Moreover, owing to the terminal amino group, ALN can be easily modified to be utilized as not only a bioactive agent but also a hydrogel network component [16,17]. But the mechanism to enhance the mechanical properties of HGM hydrogel by adding ALN remains unsolved.

The bisphosphate groups grafted to the hydrogel network, introduced by the comonomer acrylate alendronate (Ac-ALN), can strongly chelate with Ca^{2+} and Mg^{2+} to form an additional physical crosslinking [18,19] except the host-guest interaction-based crosslinking between the β-CD of the dynamic chains and the aromatic groups of gelatin polymers; this property can effectively improve the hydrogel's mechanical properties. Moreover, Mg^{2+} plays a multifunctional role in bone regeneration by contributing to the migration and tube formation of vascular endothelial cells, as well as promoting osteogenic differentiation of stem cells [20]. Additionally, Ca^{2+} also induces osteoblast migration, proliferation, and osteogenic differentiation by activating the calcium-sensitive receptor--directed signaling pathways [21]. Therefore, the introduction of Ca^{2+} and Mg^{2+} into hydrogels not only increases their mechanical properties but also effectively improves their bone repair ability.

Herein, we developed an updated ALN-Ca^{2+}/Mg^{2+}-doped supramolecular (CMS) hydrogel based on our previous HGM hydrogel by adding Ac-ALN as a comonomer (Scheme 1a). Here, the bisphosphate groups grafted to the hydrogel network introduced by the comonomer Ac-ALN strongly chelated with Ca^{2+} and Mg^{2+} to form a new kind of physical crosslinking based on the metal ion-bisphosphate coordination. In this way, we could realize the fabrication of two physical crosslinking-based CMS hydrogel only by one step of convenient photocrosslinking. Through the synthetic effect of the host-guest interaction and the metal ion-ligand coordination, the mechanical properties of this new CMS hydrogel were significantly enhanced compared with the previous HGM hydrogel based on pure host-guest interaction. At the same time, because both of these two crosslinking were reversible, the CMS hydrogel also showed injectable and self-healing properties similar to HGM hydrogel. Moreover, the efficient loading of bioactive molecular ALN and metal ions Ca^{2+}/Mg^{2+} inside CMS hydrogel was also reached during the hydrogel formation, which could trigger stem cell differentiation toward osteogenesis and further promote the therapeutic effect of in-situ repair of bone defects. Furthermore, due to the reversible crosslinking, the CMS hydrogel was able to support the migration and infiltration of endogenous cells to accelerate the formation of new bone (Scheme 1b). In short, the combination of HGM based crosslinking with metal ion-ligand coordination significantly improved the mechanical property and bioactivity of our previous HGM hydrogel. Our further *in vitro* and *in vivo* results strongly proved the feasibility of our design and this study will lay the foundation for the clinical translation of tissue engineering techniques for treating bone defects.

2. Materials and methods

2.1. Preparation of materials and animals

Gelatin, 2-hydroxy-4'-(2-hydroxyethoxy)-2-methylpropiophenone (I2959), 4′, 6-diamidino-2-phenylindole, 3-(trimethoxysilyl) propyl methacrylate, silver nitrate, paraformaldehyde, Triton X-100, sodium thiosulfate, triethyl amine (TEA), ethidium bromide, and hyaluronidase were bought from Sigma-Aldrich. β-CD, ALN, calcium chloride dihydrate ($CaCl_2{\cdot}2H_2O$), acryloyl chloride, absolute ethanol, N, N-dimethylformamide, triethanolamine (TEOA), and N-acryloxysuccimide, were purchased from Shanghai Macklin Biochemical Co., Ltd. (Shanghai, China). Magnesium chloride hexahydrate ($MgCl_2{\cdot}6H_2O$), acetone, and sodium hydroxide (NaOH) were purchased from Sinopharm Chemical Reagent Co., Ltd. (Shanghai, China). Dimethyl formamide (DMF), dimethylsulfoxide, acetone, hydrochloric acid (HCl), BCA protein assay kit, calcium, and magnesium colorimetric assay kit, and revertAid First strand cDNA synthesis kit were purchased from Fisher Scientific. Poly (ethylene glycol) diacrylate was purchased from Jenkem. Dulbecco's phosphate-buffered saline (DPBS), Dulbecco's modified Eagle's medium (DMEM), penicillin, streptomycin, L-glutamine, calcein AM dye, fetal bovine serum (FBS), and Trizol were obtained from Gibco. Peroxidase substrate kit DAB and Vectastain ABC kit were purchased from Vector Lab (CA, USA).

Thirty male Sprague-Dawley albino rats (SD rats, 8 weeks old, weighing 150–180 g) were purchased from Shanghai Jiagan Breeding Factory (Shanghai, China). All experimental animals were treated according to the standard guidelines approved by the Shanghai Jiao Tong University School of Medicine, China.

2.2. Synthesis of acrylated β-cyclodextrin (Ac-β-CD)

First, 10 g β-CD was dissolved in 150 mL DMF at room temperature. Then, the β-CD/DMF solution was cooled down to 0 °C in an ice bath, 7.2 mL TEA was added as the acid-binding agent to the mixed solution, and finally, 6 mL acryloyl chloride was added dropwise to the above solution with continuous stirring for 8 h at approximately 0 °C. The reacted solution was filtered to remove the precipitate TEA-HCl. The obtained clear solution was concentrated under reduced pressure to approximately 5–8 mL and then precipitated by adding 500 mL of cold acetone. The collected precipitate was washed with cold acetone three times and then vacuum-dried for long-term storage. ^{1}H nuclear magnetic resonance (^{1}H NMR, Bruker, 400 MHz, Billerica, MA, USA) spectra were used to characterize the vinyl modification rate of Ac-β-CD.

2.3. Synthesis of Ac-ALN

ALN and N-acryloxysuccimide were completely dissolved in 100 mL TEOA and the pH was adjusted to 8.5 with 5 M NaOH. The reaction was allowed to proceed at room temperature for 24 h with uniform magnetic stirring. The mixture was concentrated under reduced pressure and precipitated in cold ethanol. The product Ac-ALN was collected by filtration, washed with cold ethanol, and vacuum-dried. ^{1}H NMR spectra were also utilized to test the vinyl modification rate of Ac-ALN.

2.4. Preparation of CMS hydrogels

Gelatin, Ac-β-CD, and Ac-ALN were co-dissolved in DPBS to form solution 1. Simultaneously, $CaCl_2$ and $MgCl_2$ were co-dissolved in DPBS

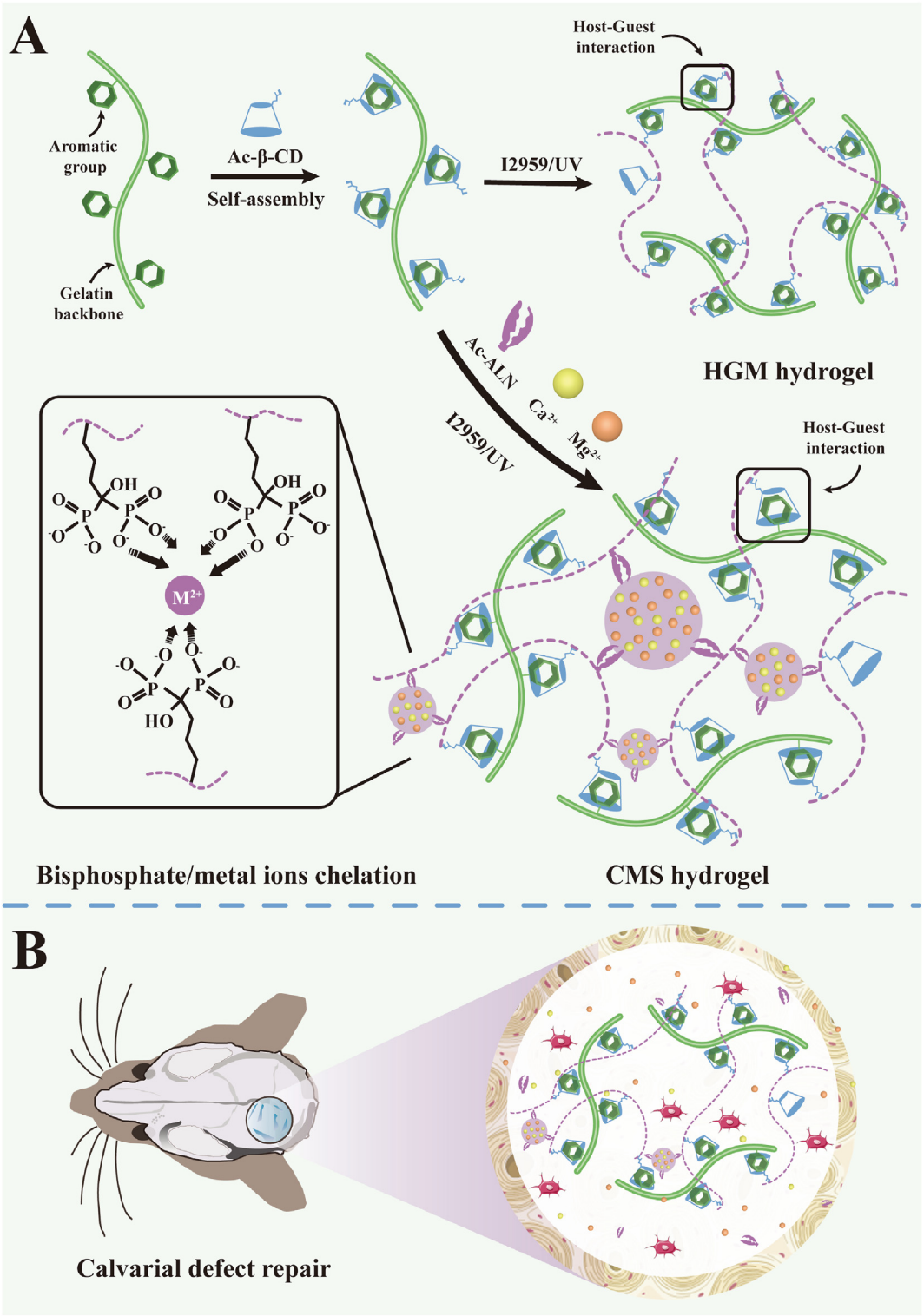

Scheme 1. Formation and application of the CMS hydrogel. Compared to the previously developed HGM hydrogel, our updated CMS hydrogel contained an additional physical crosslinking based on the chelation between the bisphosphate groups and Ca^{2+}/Mg^{2+} ions (A). After implantation into the calvarial defect, the CMS hydrogel was able to release Ca^{2+} and Mg^{2+} ions and support the migration and infiltration of endogenous cells to promote new bone regeneration (B).

to form solution 2 (Ca:Mg = 5:3). I2959 was dissolved in boiling deionized water at 0.5% to form solution 3. Solutions 1–3 were mixed in a specific proportion and then exposed to 365 nm ultraviolet (UV) light for 10 min to form the CMS hydrogel. For all CMS groups, the final concentrations of gelatin, Ac-β-CD, and I2959 were fixed at 16%, 7%, and 0.05%, respectively. The final concentrations of Ac-ALN and Ca^{2+}/Mg^{2+} ions were regulated. We used CM_xS to distinguish different groups, wherein x represented the concentrations of Ac-ALN, Ca^{2+}, and Mg^{2+} in millimolar. For example, the $CM_{100}S$ group represented the CMS hydrogel containing 100 mM Ac-ALN and 100 mM Ca^{2+}/Mg^{2+}.

2.5. Morphology of the hydrogels

To observe its microstructure, the CMS hydrogel was quenched in liquid nitrogen and split into two to expose the intersecting surface and then freeze-dried. The prepared samples were observed using cryo-field emission scanning electron microscopy (SEM, Phenomenon LE, Netherlands). Energy disperse spectroscopy (EDS) was used to test the content of the doped Ca^{2+} and Mg^{2+} simultaneously.

2.6. Equilibrium swelling studies

To test the swelling kinetics of the CMS hydrogels, the cylindrical hydrogel samples (dia = 8 mm, ht = 1 mm) were prepared in advance and the initial weights were recorded as W_0. The samples were then immersed in DPBS at pH 7.4, and the mass of each wet sample (W_w) was measured after the swelling equilibrium was reached (n = 3). The swelling ratio (%) was calculated according to the equation:

$$\text{Swelling ratio } (\%) = \frac{W_w - W_0}{W_0} \times 100\%$$

2.7. In vitro degradation

The hydrogels were formed into 8 mm diameter cylinders with volumes of 100 μL as test samples and freeze-dried to obtain the dry weights (W_a). The hydrogel samples were then placed in a 3 U/mL trypsin solution, individual samples removed at different times, freeze-dried, and weighed for the dry weight (W_b). The degradation ratio was calculated by the following equation:

$$\textit{Degradation ratio} = \frac{W_b}{W_a} \times 100\%$$

2.8. Sustained release of Ca^{2+} and Mg^{2+}

To investigate the sustained release kinetic of Ca^{2+} and Mg^{2+} from the CMS hydrogel, the prepared CMS hydrogels (n = 3) were immersed in a 3 U/mL trypsin solution at 37 °C. The soaking solution was collected at different intervals (0, 2, 4, 8, 16, 24, 72, and 120 h) and measured using an Optima 8000 inductive coupled plasma emission spectrometer instrument (Perkin Elmer). The standard ion solutions (1 mM, 2.5 mM, 5 mM, 7.5 mM, and 10 mM) were prepared for the standard curve.

2.9. Rheological measurements

The rheological properties of the hydrogels were tested at room temperature using an Ares G2 TA rheometer (DE, USA) with an 8 mm diameter parallel plate and a 1 mm gap. A time sweep was performed at a fixed frequency of 6 rad/s and strain of 1%. As for the frequency sweep, the strain was fixed at 1% and the frequency ranged from 0.5 to 500 rad/s. A strain sweep was performed at a fixed frequency of 6 rad/s and a strain range from 1% to 500%. To determine the self-healing and injectable properties of the CMS hydrogel, the time sweep was further measured under alternative low-high strain (1%–300%).

2.10. Self-repair performance testing

The prepared CMS hydrogels of different shapes were dyed yellow or blue with methyl orange or methylene blue, respectively. Then, the rounded and the pentagram-shaped hydrogels were cut into two pieces, and then these hydrogels were spliced into new shapes at 37 °C for 5 min.

2.11. Compressive and tensile testing

The compressive strain-stress curves were tested with hydrogels (diameter: 5 mm, height: 3 mm) at a speed of 0.03 mm/s. As for the cyclic compressive test, the speed was also fixed at 0.03 mm/s and the maximum strain was fixed at 50%. For the tensile test, the hydrogel samples (length: 5 mm, thickness: 1.5 mm) underwent a tensile speed of 0.05 mm/s.

2.12. Cell harvest and culture

Bone marrow-derived stem cells (BMSCs) were isolated from SD rats. Briefly, harvested BMSCs were washed, centrifuged, and resuspended in DMEM supplemented with 10% FBS and 100 U/mL penicillin. The medium was replaced every 2 days until the primary cells reached a confluence of approximately 80%. Then, the cells were trypsinized with 0.25% trypsin and subcultured at a density of 1×10^4 cells/mL. BMSCs at passage 2 (P2) were used for further experiments.

2.13. Cytocompatibility of CMS hydrogels

The P2 BMSCs were seeded onto different CMS hydrogel groups (control, CM_0S, $CM_{100}S$, $CM_{200}S$, and $CM_{300}S$ groups) at a density of 1.0×10^5 cells/mL and cultured *in vitro* for 4 days. The viability of BMSCs in the hydrogels was determined using the live/dead cell viability assay (Yeasen Biotechnology, Shanghai, China) followed by an examination under a Nikon confocal microscope (Tokyo, Japan). To directly analyze the morphological features of BMSCs within hydrogels, the cytoskeleton was stained with phalloidin (Sigma) for 1–4 days. The Cell Counting Kit-8 (CCK-8) was used to evaluate the proliferation of BMSCs within the hydrogels at 1 and 4 days.

2.14. In vitro osteogenic bioactivity of CMS hydrogels

To evaluate the osteogenic capacity of CMS hydrogels, P2 BMSCs were suspended at a final concentration of 5×10^6 cells/mL, and 200 μL of the cell suspension was evenly encapsulated into various CMS hydrogels (control, CM_0S, $CM_{100}S$, $CM_{200}S$, and $CM_{300}S$ groups) and cultured in the osteogenic medium (DMEM with 16.7% FBS, 1% penicillin, 1% L-glutamine, 10 mM β-glycerophosphate disodium, 50 mg/mL L-ascorbic acid 2-phosphate sesquimagnesium salt hydrate, and 100 nM dexamethasone) for 21 days. To determine extracellular matrix mineralization, calcium deposition in the samples was examined using alizarin red S staining at 10 days post-seeding.

In addition, ALN, Ca^{2+}, Mg^{2+}, Ca^{2+}/Mg^{2+}, and ALN + Ca^{2+}/Mg^{2+} were individually embedded into HGM hydrogels to achieve a final 100 mM concentration. Thereafter, these hydrogels were cocultured with BMSCs and subjected to *in vitro* culture in the osteogenic medium for 10 days.

Western blot (WB) analysis was used to detect the expression of osteogenesis-related proteins, including alkaline phosphatase (ALP), collagen I, and osteocalcin (OCN). Total cell homogenates were boiled with SDS–PAGE sample buffer for 5 min. Protein content in all fractions was determined using a protein assay kit (Pierce Coomassie). Equal amounts of protein (40 μg) from all fractions (depending on the target) were separated on different percentages of SDS–PAGE gels, transferred to nitrocellulose membranes, and incubated with primary antibodies. Then, each membrane was washed and incubated with the secondary antibody for an additional 2 h. All antibodies were prepared in the washing buffer Tris-buffered saline-Tween 20 (Gibco) and incubated for 2 h at room temperature with shaking. Antigen antibody interactions were detected using ECL reagents (Pierce). Images were scanned and analyzed using a C-Di Git blot scanner and software.

The enzyme-linked immunosorbent assay (ELISA) was performed using ALP, collagen I, and OCN ELISA kits (Abcam) to measure the expression levels of osteogenesis-related protein according to the manufacturer's protocol.

At 10- and 21-days, samples were collected to analyze the expression

Table 1
Primer sequences.

Gene	Primers	
	Forward (5′–3′)	Reverse (5′–3′)
Collagen I	CTGCCCAGAAGAATATGTATCACC	GAAGCAAAGTTTCCTCCAAGACC
OCN	CAAAGGTGCAGCCTTTGTGTC	TCACAGTCCGGATTGAGCTCA
Runx-2	CCTTCCACTCTCAGTAAGAAGA	TAAGTAAAGGTGGCTGGATAGT
β-actin	ATCATGTTTGAGACCTTCAA	CATCTCTTGCTCGAAGTCCA

of osteogenic genes (collagen I, OCN, and Runt-related transcription factor 2 [Runx-2]). Real-time-polymerase chain reaction (RT-PCR) was conducted (Applied Biosystems 7300 RT-PCR system, MA, USA) using Taqman primers and probes specific for osteogenic genes, with housekeeping gene β-actin for normalization, as previously reported [22]. Primer sequences are listed in Table 1.

2.15. Tube formation assay

An *in vitro* tube formation assay was performed using Matrigel (BD Bioscience) according to the manufacturer's specifications. Human umbilical vein endothelial cells (HUVECs) were purchased from the Type Culture Collection of the Chinese Academy of Sciences and seeded into 24-well plates coated with Matrigel, and four types of hydrogels were added. After a 6 h incubation, the HUVECs were imaged using a light microscope.

2.16. In vivo cranial regeneration

Thirty SD rats were randomly divided into five groups (n = 6): control, CM_0S, $CM_{100}S$, $CM_{200}S$, and $CM_{300}S$ groups. For each rat, two 5 mm diameter craniotomy defects were created at the parietal bones of the skull on each side of the sagittal suture line using a 5 mm diameter trephine bur. Next, the various groups of CMS hydrogels were injected

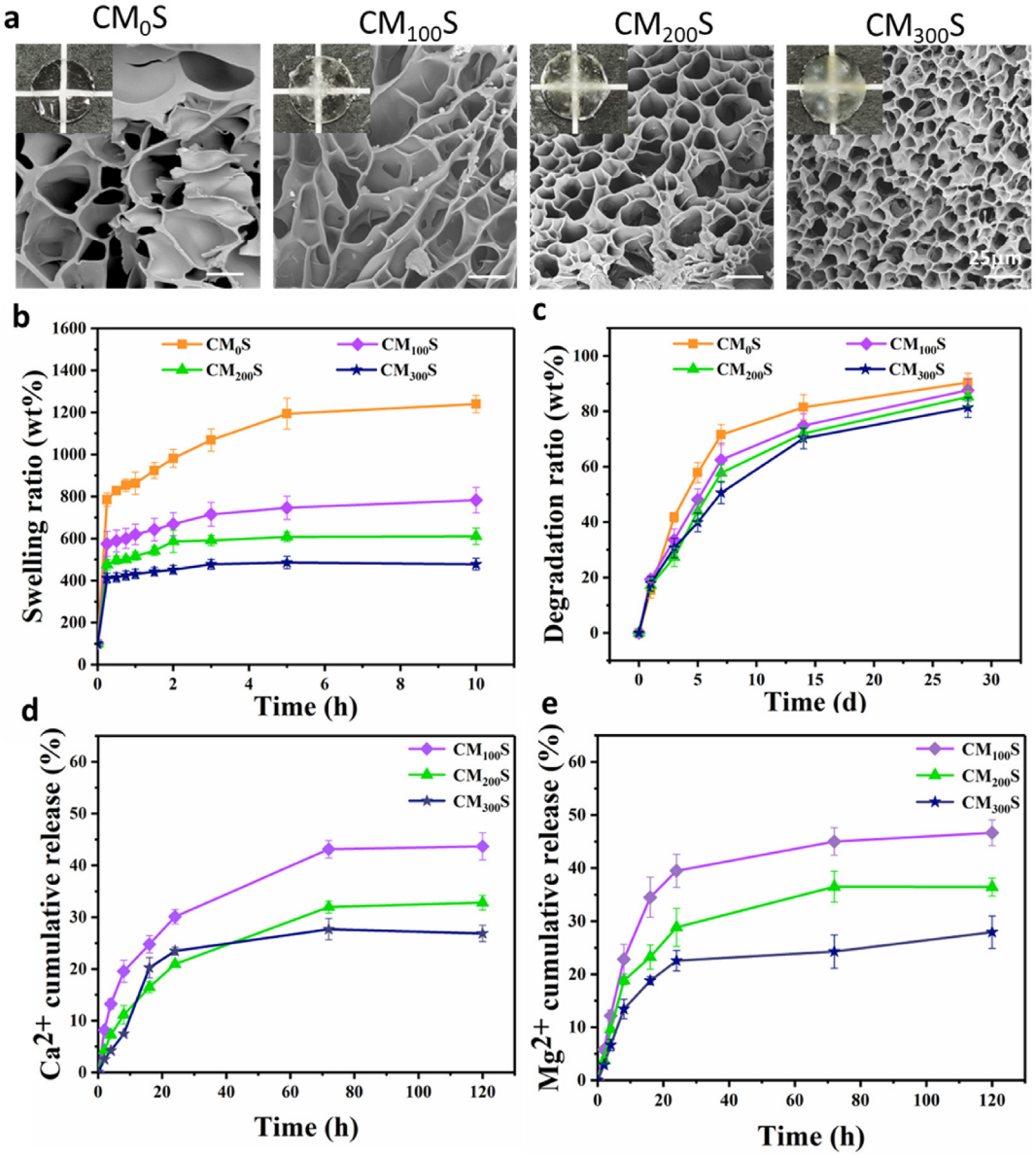

Fig. 1. Characterizations of the different CMS hydrogels. (a) The SEM images of CMS hydrogel with different concentrations of Ac-ALN and Ca^{2+}/Mg^{2+} (CM_0S group: without Ac-ALN and Ca^{2+}/Mg^{2+}; $CM_{100}S$ group: 100 mM Ac-ALN and 100 mM Ca^{2+}/Mg^{2+}; $CM_{200}S$ group: 200 mM Ac-ALN and 200 mM Ca^{2+}/Mg^{2+}; $CM_{300}S$ group: 300 mM Ac-ALN and 300 mM Ca^{2+}/Mg^{2+}), the inner pictures are the photos of the prepared CMS hydrogels. (b) The swelling behavior of CMS hydrogels. (c) The degradation measurement of CMS hydrogels with 3 U/mL trypsin at 37 °C. The long-term release of Ca^{2+} (d) and Mg^{2+} (e) from CMS hydrogels at 37 °C.

into the defect sites of the rats, followed by UV irradiation for 10 min; no hydrogel was administered to the rats in the control group. At 6 or 12 weeks after surgery, the rats were sacrificed for evaluation.

To evaluate the qualitative and quantitative cranial regeneration level, a high-resolution microtomography scanner (Scanco μ-80) was used to visualize the defects in the harvested samples at 12 weeks. Bone regeneration was measured as bone volume per tissue volume (BV/TV) and bone mineral density (BMD). A threshold of 22% (220 on a grayscale of 0–1000) was used to segment bone from non-bone to quantify bone volume.

To evaluate angiogenesis, Microfil (Carve)-perfused rats were used. Micro-CT (Skyscan 1176, Belgium) analysis was then performed, setting the resolution to 9 μm. Finally, the vessel volume was calculated and subjected to statistical analyses.

For histological analysis, the samples at 6 and 12 weeks after surgery were stained with hematoxylin & eosin (H&E), Masson's trichrome, and collagen I staining to assess the regenerated bone tissue.

2.17. Statistical analysis

The results of the experiments were statistically analyzed using SPSS version 19.0 software. All data are presented as mean ± standard deviation (SD) and were analyzed via one-way analysis of variance (ANOVA) with $^*p < 0.05$ as the significance threshold.

3. Results and discussion

3.1. Preparation of CMS hydrogels

The present study developed an upgraded supramolecular CMS hydrogel based on our previously fabricated HGM and aimed at improving the mechanical properties and osteogenic bioactivity for use in bone regeneration. The CMS hydrogel was prepared by adding a new physical crosslinking comprising the strong chelation of the comonomer Ac-ALN and Ca^{2+}/Mg^{2+} to the HGM hydrogel.

To prepare the CMS hydrogel, we initially synthesized two kinds of comonomers: Ac-β-CD and Ac-ALN. As shown in the ^{1}H NMR spectrum (Fig. S1a), there were significant double bond peaks present around chemical shifts 6.2–6.3 ppm, indicating that the β-CD had been successfully acrylated, and the average degree of acrylate substitution was calculated as 1 based on the area integral to the characteristic peaks, i.e., one double bond was modified for each β-CD molecule. As for the Ac-ALN, the peaks for carbon double bond could be observed in the range of chemical shifts around 6.2 ppm (Fig. S1b). The average degree of acrylate substitution should be 0.75, indicating that 75% of the initial ALN was grafted to the acrylated groups. During the synthetic process, we did not remove the remaining 25% of unmodified ALN, and this part of ALN was also included in the hydrogel formation through the chelation of the bisphosphate groups of ALN and the Ca^{2+} and Mg^{2+} ions (Scheme 1a). To simplify the representation, we used the concentration of Ac-ALN to represent the total concentration of the modified and unmodified ALN.

For the CMS hydrogels fabrication, we first prepared three solutions, as described in the Methods section. Specifically, in solution 1, the small molecule Ac-β-CD would be self-assembled with the natural polymer gelatin through the host-guest complex formation between the hydrophobic cavities of Ac-β-CD and the aromatic groups of the gelatin backbone (Scheme 1a). The above solutions were mixed in a special ratio to form the precursor solutions of CMS hydrogels. During this process, another self-assembling formation was based on the chelation between

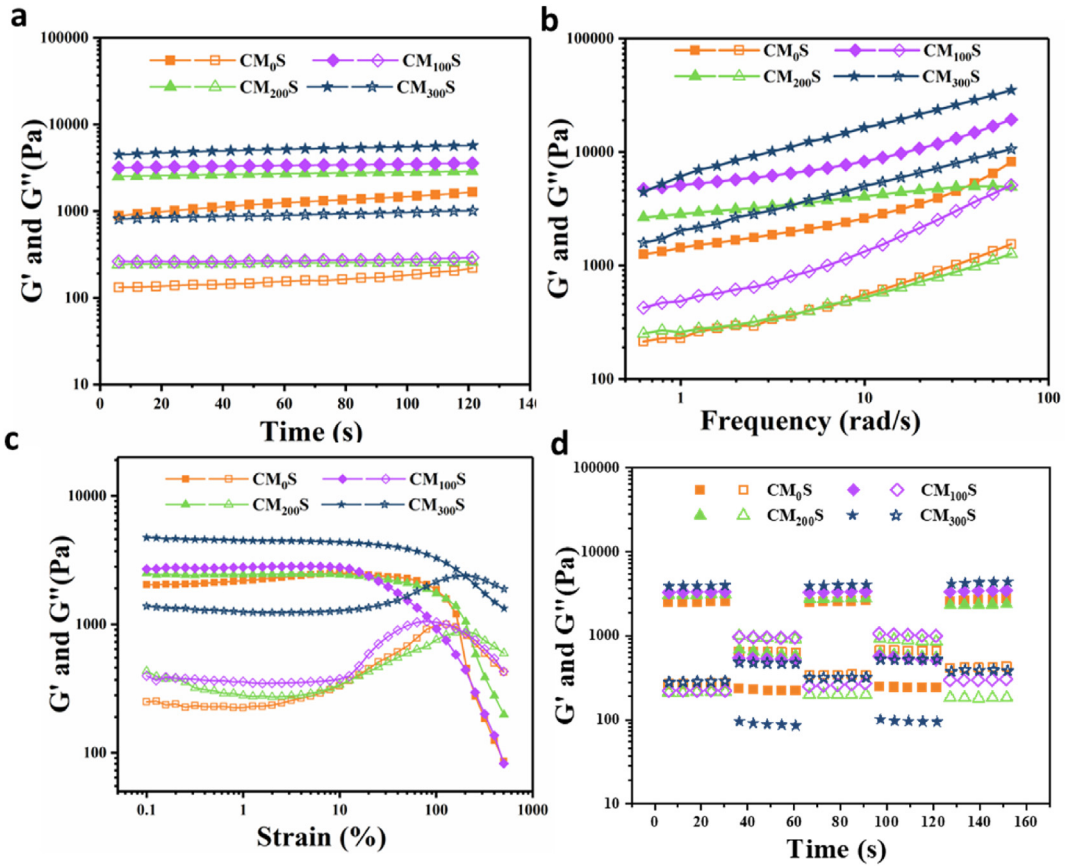

Fig. 2. Rheological properties of the different CMS hydrogels. (a) The time sweep test under a fixed frequency of 6 rad/s and strain of 1%; (b) The frequency sweep test at a fixed strain of 1% and range frequency of 0.5–500 rad/s; (c) The strain sweep test at a fixed frequency of 6 rad/s and range strain of 1%–500%; (d) Alternative low-high strain sweep at a low strain of 1% and high strain of 300%.

the bisphosphate groups of Ac-ALN and the Ca^{2+}/Mg^{2+} ions. Then, the prepared precursor solution was exposed to UV (365 nm) for 10 min to form the gelatinized CMS hydrogel through radical polymerization among the vinyl groups of Ac-β-CD and Ac-ALN. For all CMS groups, the final concentrations of gelatin, Ac-β-CD, and I2959 were fixed at 16%, 7%, and 0.05%, respectively. The final concentrations of Ac-ALN and Ca^{2+}/Mg^{2+} ions were regulated, and we used CM_xS to distinguish different hydrogel groups, wherein x represents the final concentration of Ac-ALN and Ca^{2+}/Mg^{2+} ions in millimolar. As shown in Scheme 1a, CMS hydrogel was structured with two kinds of physical crosslinking, namely the host-guest interaction and the metal ion-ligand coordination. Therefore, compared to the previous HGM hydrogel, the updated CMS hydrogel was expected to present better mechanical properties while maintaining similar dynamic properties like self-healing properties.

3.2. Characterization of CMS hydrogels

After the successful preparation of CMS hydrogels, we observed that the gelatigenous CMS hydrogels gradually turned milky white with increasing concentrations of Ac-ALN and Ca^{2+}/Mg^{2+} (Fig. 1a). This phenomenon intuitively indicated the formation of the metal ion-ligand coordination between the Ca^{2+}/Mg^{2+} ions and the bisphosphate groups of Ac-ALN as the second crosslinking inside the CMS hydrogels. The homogeneous connected porous microstructure of CMS hydrogels was also shown by the SEM in Fig. 1a, which demonstrated that the higher concentration of Ac-ALN and Ca^{2+}/Mg^{2+} led to a denser network structure with smaller pore sizes in CMS hydrogels. Additionally, the EDS analysis in Fig. S2 revealed the wide distribution of Ca^{2+} and Mg^{2+} within the CMS hydrogel. These data proved the successful introduction of the metal ion-ligand coordination between the bisphosphate groups of Ac-ALN and Ca^{2+}/Mg^{2+} and this secondary crosslinking greatly increased the crosslinking density of CMS hydrogel as intended, which was the foundation of the mechanical strength enhancement of CMS hydrogels. Before the mechanical property measurement, we tested the swelling and degradation behavior of CMS hydrogels. As shown in Fig. 1b, although the swelling behaviors of all CMS hydrogels were similar, the swelling ratio and final swelling equilibrium ratio of each group were quite different, which also depended on the concentration of Ac-ALN and Ca^{2+}/Mg^{2+}. Among the four CMS hydrogel groups, $CM_{300}S$ hydrogel had the lowest swelling ratio because it had the densest crosslinking. Similar to the swelling behavior, the degradation rate of CMS hydrogel also decreased with the increase of Ac-ALN and Ca^{2+}/Mg^{2+} concentration (Fig. 1c). This result was anticipated because a high crosslinking density favors the maintenance of the integrity of hydrogels. Furthermore, we focused on the long-term release of Ca^{2+} and Mg^{2+} from CMS hydrogel. The releasing kinetics of both $Ca^{2+}$and Mg^{2+} was divided into three stages: (1) 0–12 h with a rapid release speed: Ca^{2+} or Mg^{2+} that were not tightly bound to the bisphosphate groups underwent a burst release; (2) 12–24 h with a medium release speed: Ca^{2+} or Mg^{2+} that were bound to the bisphosphate groups of dissociative ALN underwent a constant moderate release; and (3) after 24 h with a low release speed: Ca^{2+} or Mg^{2+} that were bound to the bisphosphate groups of the grafted

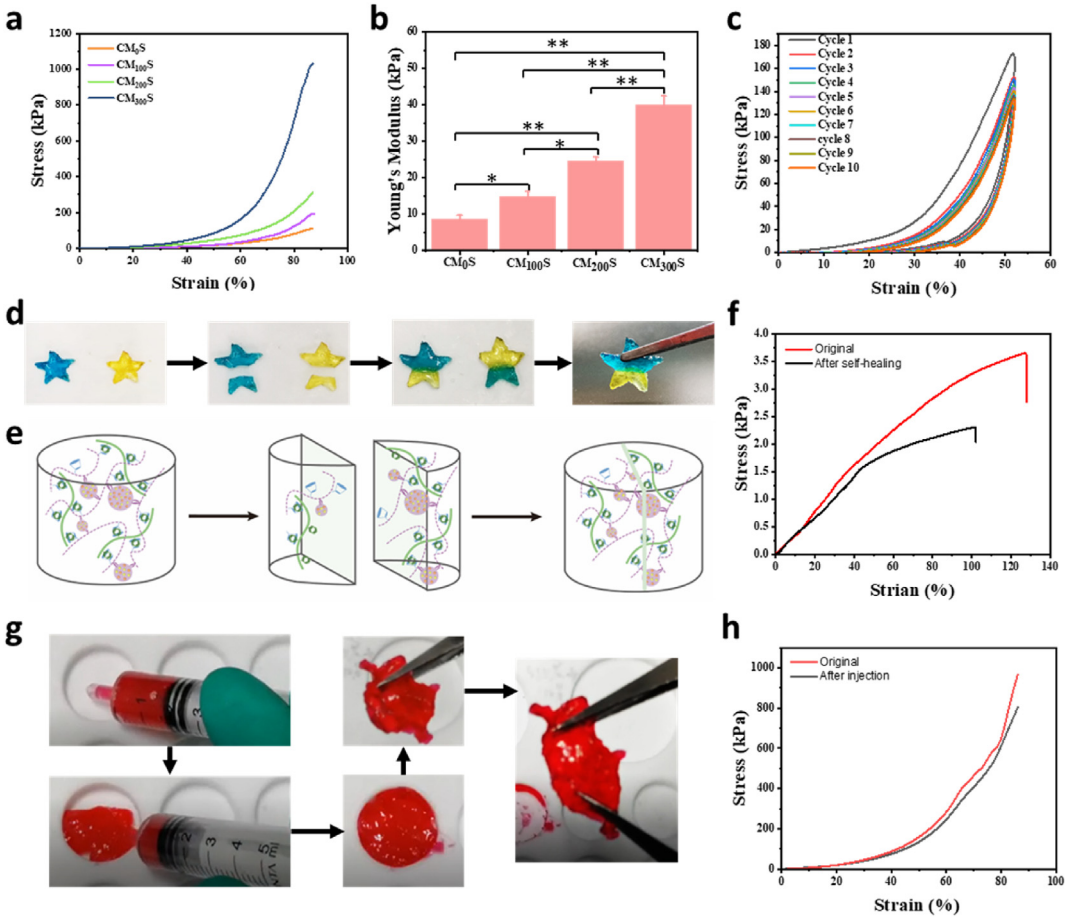

Fig. 3. Mechanical properties of CMS hydrogels. (a) The compressive strain-stress curves of CMS hydrogels. (b) The compressive Young's Modulus of CMS hydrogels. (c) The cyclic compressive strain-stress curves of $CM_{300}S$ hydrogel. (d) The self-healing demo of $CM_{300}S$ hydrogel. (e) The scheme for the self-healing progress of CMS hydrogel. (f) The tensile strain-stress curves of $CM_{300}S$ hydrogel before and after self-healing. (g) The injection demo of $CM_{300}S$ hydrogel. (h) The compressive strain-stress curves of $CM_{300}S$ hydrogel before and after injection. $^*P < 0.05$. $^{**}P < 0.001$.

ALN on the hydrogel network underwent a slow release (Fig. 1d–e). We hypothesized that this Ca^{2+}/Mg^{2+}-releasing characterization of our CMS hydrogel was suitable for its application as a bone regenerative scaffold [23–26]. We speculated that after the CMS hydrogel filled the bone defects, the early burst release of Ca^{2+}/Mg^{2+} would help to create a suitable microenvironment for rapid bone regeneration; next, the subsequent constant release of Ca^{2+}/Mg^{2+} would trigger the osteogenesis of the pre-loaded and infiltrated BMSCs; and finally, the slow release of Ca^{2+}/Mg^{2+} would provide a long-term conductive microenvironment to the bone regeneration.

Next, we tested the rheological properties of our different CMS hydrogels. In Fig. 2a, the time sweep results demonstrated that compared to CM_0S hydrogel, the storage moduli of $CM_{100}S$, $CM_{200}S$, and $CM_{300}S$ hydrogel increased considerably, although the different in storage moduli among the different CMS groups was in significant. This data proved that the metal ion-ligand coordination between Ca^{2+}/Mg^{2+} and bisphosphate groups as the newly introduced crosslinking improved the mechanical property of CMS hydrogel compared to our previous HGM hydrogel (CM_0S group). As for the insignificant difference among the $CM_{100}S$, $CM_{200}S$, and $CM_{300}S$ groups, we speculated that it was because the further increase of the Ac-ALN and Ca^{2+}/Mg^{2+} concentration favored the increase in the size of the metal ion-ligand coordination instead of the number. The following frequency sweep data in Fig. 2b clearly shows the frequency dependence of the hydrogel modulus, which is strong evidence for the reversible physical crosslinking of CMS hydrogels. The strain sweep indicated that the breaking strain for all the CMS hydrogel groups was approximately 100–200% (Fig. 2c); hence, we chose 300% as the high strain for the following alternative low-high strain sweep test. The result in Fig. 2d shows that all the CMS hydrogels have good shear-thinning properties and the modulus recovery ratio reaches 100%; this further proved that two kinds of crosslinking existed inside our CMS hydrogels, namely the host-guest complexation between the β-CD cavities and aromatic groups of gelatins and the metal ion-ligand coordination between Ca^{2+}/Mg^{2+} and bisphosphate groups of ALN, were reversible physical crosslinking.

Next, we observed the mechanical properties of our CMS hydrogel *via* a compressive test. As shown in Fig. 3a, all CMS hydrogel groups underwent over 80% compressive strain without being destroyed. The

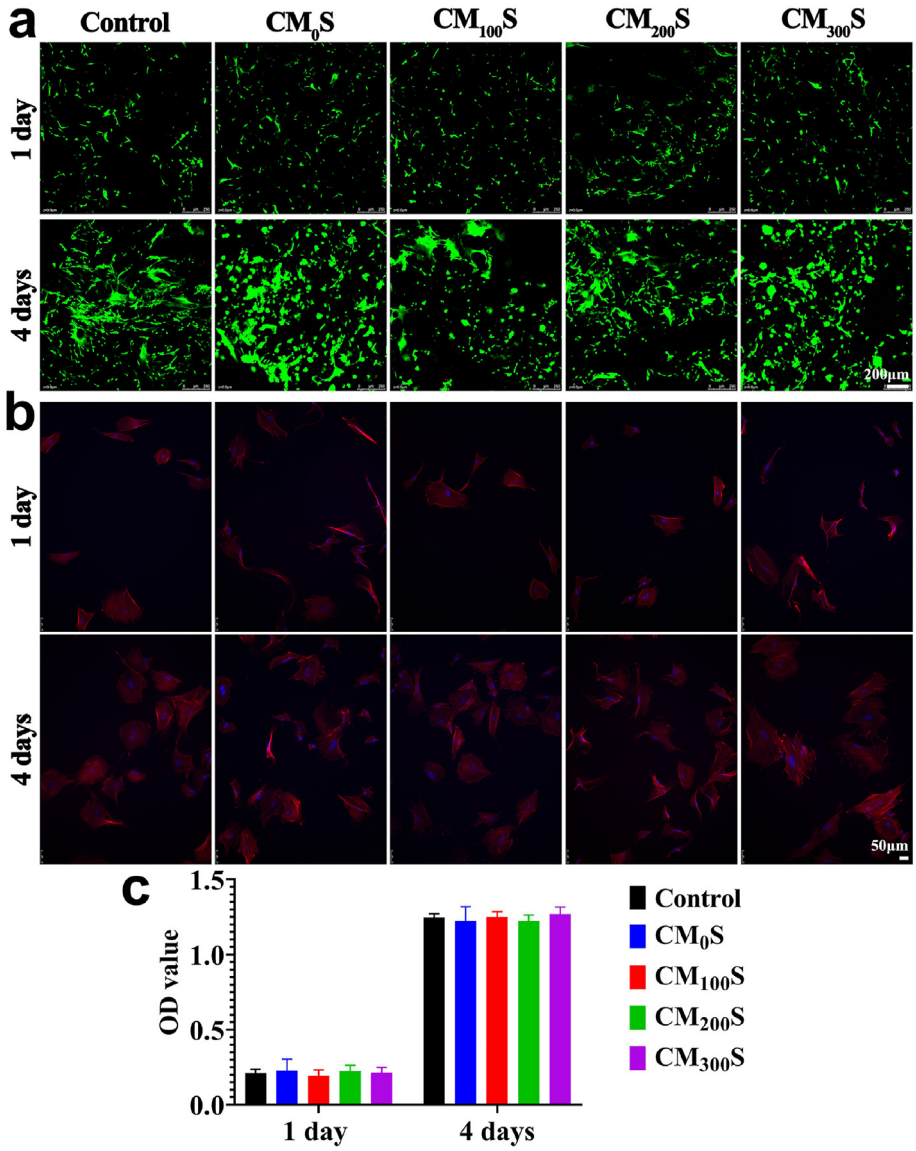

Fig. 4. Biocompatibility of the different CMS hydrogels with BMSCs at 1 and 4 days. (a) Live/dead staining, in which live cells are stained with green color and dead cells are stained with red color; (b) Phalloidin staining, in which nucleus is stained with blue color and cytoskeleton is stained with red color; (c) OD value via CCK-8 assay.

compressive Young's modulus of CMS hydrogels increased with the increase in ALN and Ca^{2+}/Mg^{2+} concentration. This result was consistent with our rheological data, which also proved that the introduction of Ca^{2+}/Mg^{2+} coordination as the second crosslinking in CMS hydrogel improved the mechanical strength of the hydrogel (Fig. 3b). We used $CM_{300}S$ hydrogel as the representative of CMS hydrogel for the following test. The cyclic compressive test showed that our CMS hydrogel dissipated energy well during the repeating compressive progress (Fig. 3c). This probably contributed to the reversible crosslinks in CMS hydrogel that could be easily unlocked under force and recovered without force. Because of the reversible crosslinks, our CMS hydrogels are also self-healable. For example, two pentagram-shaped CMS hydrogels (blue and yellow) that were cut into two pieces were able to form two new intact hydrogels within several minutes simply by bringing the two cross-sections of the CMS hydrogels in close contact (Fig. 3d and **Video 1**). This is because of the efficient reformation of the reversible host-guest interaction and metal ion-ligand coordination between the two cross-sections (Fig. 3e). Furthermore, the tensile test of CMS hydrogel before and after self-healing showed that after 1 h of self-healing, the breaking strain of CMS hydrogel recovered to 86% of its original state and the tensile Young's modulus almost recover 100% (Fig. 3f). Compared to previous studies [27,28], this self-healing property of our CMS hydrogel was also satisfactory. We believe that this efficient self-healing property of CMS hydrogel guarantees its long-term integrality after *in-situ* implantation into the bone defects [29–33]. At the same time, the reversible physical crosslinks of CMS hydrogel also endowed it with an injectable property. As shown in Fig. 3g and **Video 2**, the prepared CMS hydrogel could be reinjected to form an intact hydrogel. More importantly, the injection showed no negative effect on the mechanical property of our CMS hydrogel (Fig. 3h). This excellent injectable property made the CMS hydrogel satisfy the filling of different shape defects.

In our previous study, we proved that owing to the reversible nature of the host-guest complexation crosslinks in the supramolecular hydrogels, HGM hydrogels displayed superior support for cell infiltration and migration without undergoing structural damage [10]. However, the host-guest interaction between the aromatic residues of gelatin and β-CD, which is the sole crosslinking mechanism in HGM hydrogels, is too weak to meet the mechanical property requirements of hydrogels for in-situ bone defect repair. To resolve this problem, in this study, we introduced a new physical crosslinking in the HGM hydrogel and pioneered the CMS hydrogel. There are two main reasons why we chose physical crosslinking. Firstly, compared to the chemically crosslinked hydrogels, which are well-known for their good mechanical properties, the physically crosslinked hydrogels prevent toxicity due to the residual initiator and the unreacted chemical crosslinkers [34]. Furthermore, according to the mechanical property test results in this study, the secondary physical crosslinking of Ac-ALN and Ca^{2+}/Mg^{2+} distinctly improved the mechanical properties of the supramolecular hydrogel, which compensated for the weak mechanical property of this physically crosslinked hydrogel. Second, continuing to use physical crosslinking to enhance the mechanical properties of HGM hydrogel did not damage its original structure; moreover, the updated CMS hydrogel is also self-healable and injectable as the HGM hydrogel, which was confirmed by the above results.

3.3. Cytocompatibility of CMS hydrogels

To evaluate the cytocompatibility of CMS hydrogels, BMSCs were encapsulated into different hydrogels (CM_0S, $CM_{100}S$, $CM_{200}S$, and $CM_{300}S$ groups) and cultured *in vitro* culture for 4 days. The BMSCs in all

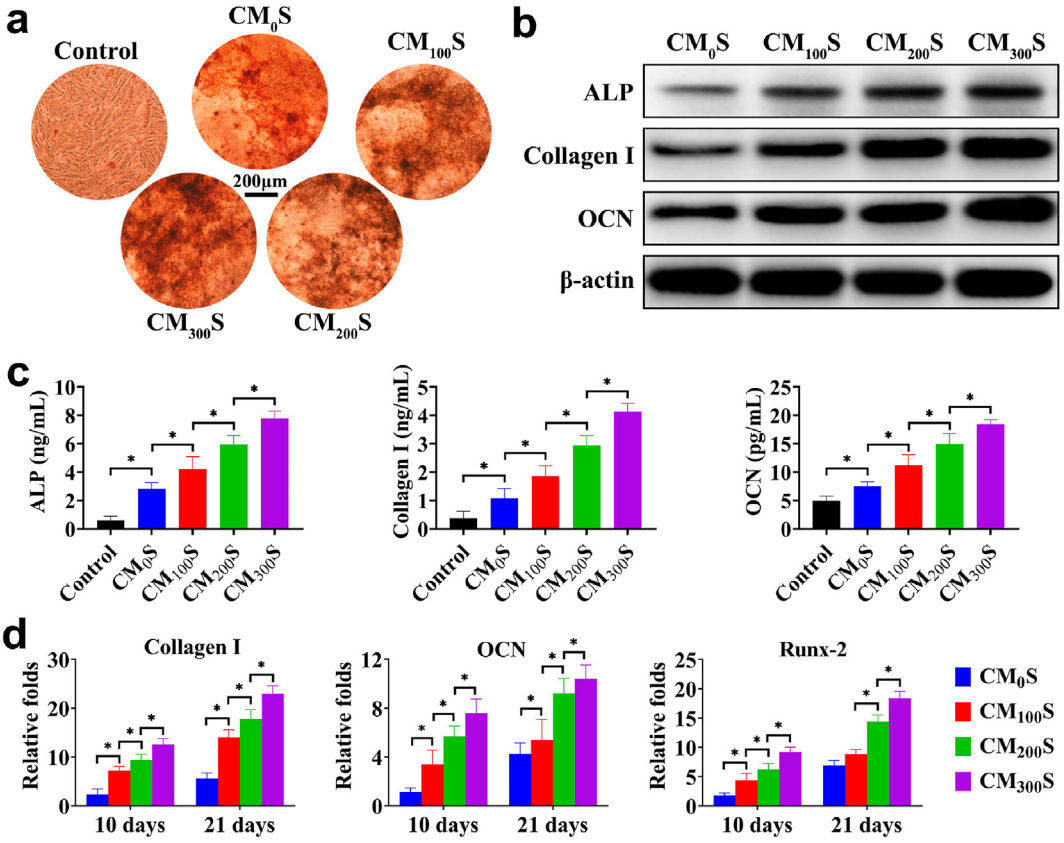

Fig. 5. ***In vitro*** **osteogenic evaluation of BMSCs within the different CMS hydrogels.** (a) Alizarin Red S staining in various hydrogels at 10 days; Expression of osteogenic proteins (ALP, collagen I, and OCN) via WB (b) and ELISA (c) examinations at 10 days; (d) Expression of osteogenic genes (collagen I, OCN, and Runx-2) via RT-PCR examination at 10 and 21 days. $^*P < 0.05$.

CMS hydrogels showed similar viability as the control group, and few dead cells were visible over 1–4 days as evaluated by live/dead staining (Fig. 4a). Notably, BMSCs displayed well-stretched structures and favorable viability in all the groups over the 4-day *in vitro* culture course, as indicated by phalloidin staining (Fig. 4b). The quantitative CCK-8 assay further verified that BMSC within all CMS hydrogels exhibited a favorable proliferation rate as the control group (Fig. 4c). The use of physically crosslinked hydrogels prevented toxicity due to the residual initiator and the unreacted chemical crosslinkers in chemically crosslinked hydrogels [34]. Further, the Ca^{2+}/Mg^{2+} ratio of the different CMS groups in this study was also within a suitable range as high Mg^{2+} would have exhibited an inhibitory effect on osteoblast differentiation and mineralizing activity [35]. These results suggest that all the CMS hydrogels are nontoxic and biocompatible with BMSCs.

3.4. *In vitro* osteogenic differentiation of CMS hydrogels

In addition to mechanical robustness, osteogenic differentiation capacity is another essential consideration in the development of hydrogel platforms for bone regeneration. To directly explore the osteogenic differentiation capacity of CMS hydrogels, BMSCs were encapsulated into different hydrogels (CM_0S, $CM_{100}S$, $CM_{200}S$, and $CM_{300}S$ groups). After 10 days of *in vitro* culture, samples in the different groups were stained with alizarin red S to verify calcium salt deposition. More intensive red staining of calcium nodules was observed with the increase in the concentration of Ac-ALN and Ca^{2+}/Mg^{2+} at 10 days (Fig. 5a), and samples in the $CM_{300}S$ group showed the best matrix mineralization performance. In accordance with the alizarin red S staining results, WB (Fig. 5b) and ELISA (Fig. 5c) examinations also corroborated that osteogenesis-related proteins expression (ALP, collagen I, and OCN) increased with increased Ac-ALN and Ca^{2+}/Mg^{2+} concentrations at 10 days. A quantitative analyses of osteogenesis-related genes expression (collagen I, OCN, and Runx-2) via RT-PCR (Fig. 5d) assay also showed that the expression of osteogenic genes was elevated with the increased Ac-ALN and Ca^{2+}/Mg^{2+} concentrations and prolonged time from both 10 and 21 days. Collectively, these results indicated that the incorporation of Ac-ALN and Ca^{2+}/Mg^{2+} further enhanced the osteogenic ability of the hydrogels.

Magnesium (Mg) is an important component of human bones and an essential element participating in numerous cellular, including in osteoblasts and osteoclasts, physiological functions. Mg-based scaffolds have been reported to play positive roles in BMSC-mediated osteogenesis [36]. The use of calcium phosphates to enhance bone growth has been a common practice in medicine since the 1980s and implantable polymeric scaffolding materials with calcium phosphates have been developed to effectively promote in-situ bone regeneration [37]. ALN, as a United States FDA-approved drug [11,12], also significantly promotes osteogenic differentiation. We further evaluated the synergistic effect of Ac-ALN, Ca^{2+} and Mg^{2+} in promoting osteogenesis. HGM hydrogels supplemented with ALN, Ca^{2+}, Mg^{2+}, Ca^{2+}/Mg^{2+}, and ALN +

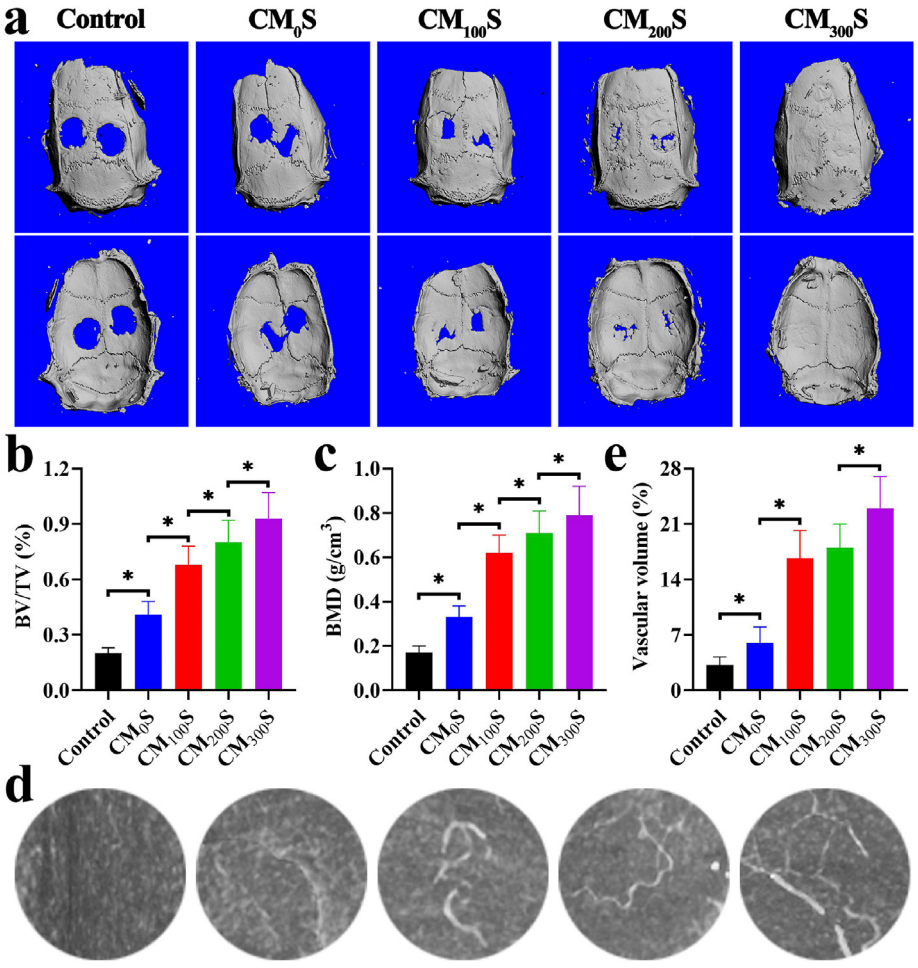

Fig. 6. Micro-computed tomography evaluation of bone regeneration with the different CMS hydrogels at 12 weeks. (a) Micro-computed tomography images of the different groups; (b–c) Quantitative evaluations of BV/TV and BMD in the different groups. (d) Angiographical images in the different groups. (e) Quantitative evaluations of vascular volume in the different groups. *$P < 0.05$.

Ca^{2+}/Mg^{2+} were cocultured with BMSCs and subjected to *in vitro* culture for 10 days. The expression of osteogenic genes (collagen I and OCN) using RT-PCR examination (Figs. S3a–b) and that of osteogenic proteins (collagen I and OCN) (Figs. S3c–d) using ELISA exhibited a similar trend: control < ALN < Ca^{2+} < Mg^{2+} < Ca^{2+}/Mg^{2+} < ALN + Ca^{2+}/Mg^{2+}, corroborating that all the Ac-ALN, Ca^{2+}, and Mg^{2+} within the hydrogel play a synergistic effect in promoting osteogenesis.

3.5. Bone regeneration in a rat cranial defect model

The different hydrogels (CM_0S, $CM_{100}S$, $CM_{200}S$, and $CM_{300}S$ groups) were subsequently used for in-situ bone repair in a rat cranial defect model. The micro-computed tomography (CT) observations (Fig. 6a) showed that the samples displayed better healing outcomes with increasing Ac-ALN and Ca^{2+}/Mg^{2+} concentrations. Notably, the defect in the $CM_{300}S$ group achieved the best therapeutic effect among all the CMS hydrogels and was almost completely repaired with a relatively smooth surface at 12 weeks post-surgery. Furthermore, the quantitative analyses of bone histomorphometric parameters, including BV/TV and BMD, showed the same trend among the CM_xS groups with the micro-CT results, and the $CM_{300}S$ group outperformed the other CMS hydrogel groups after 12 weeks (Fig. 6b–c).

Subsequently, the angiogenesis process was evaluated among the repaired samples. The white strips in Fig. 6d refer to neovascularization. The data showed that the number and volume of neovascularization were significantly enhanced with increasing Ac-ALN and Ca^{2+}/Mg^{2+} concentrations. It was reported that Mg^{2+} also showed a pro-angiogenic effect via significantly promoting angiogenesis-related gene expression [38]; therefore, we attributed this result to the favorable release of Mg^{2+} from CMS hydrogel. We further conducted an *in vitro* tube formation assay by coculturing CMS hydrogel with HUVECs for 6 h. Our results revealed that the tube formation (including branch and tube numbers) enhanced considerably with increased Ac-ALN and Ca^{2+}/Mg^{2+} concentrations (Fig. S4), thus confirming our assumption that the fabricated CMS hydrogel may promote angiogenesis through the release of Mg^{2+}.

Histopathological staining was further performed to evaluate bone regeneration stimulated by the implanted CMS hydrogels. At 6 weeks after surgery, for the control group, both H&E and Masson's trichrome staining showed an obvious hollow at the center of the defect area and the rest of the defect site was filled in with a small amount of loose fibrous tissue. Meanwhile, although none of the defects were completely repaired, every rat in the CM_xS group appeared to have a large amount of fibrous tissue filling the defect site and several islands of new bone tissue were formed inside the fibrous tissue with osteoblasts arranged around. Notably, with the increase in Ac-ALN and Ca^{2+}/Mg^{2+} concentrations, the bone repair effect showed improvement (Fig. 7a). The defects in all the groups were gradually repaired over an extended time from 6 to 12 weeks. At 12 weeks after surgery, the control group contained only a small amount of new bone tissue, whereas the CM_xS groups exhibited relatively better osteogenic effects, with enhanced osteogenic effects observed with increased Ac-ALN and Ca^{2+}/Mg^{2+} concentrations among the different CMS hydrogels. Furthermore, the regenerated bone tissues of the $CM_{300}S$ group, which almost completely and smoothly filled the defect, showed a large area of positive red H&E staining and positive green Masson's trichrome staining, achieving the most satisfactory in-situ cranial bone regeneration after 12 weeks (Fig. 7b). Immunohistochemical collagen I staining of the repaired tissue in the different CMS groups further confirmed enhanced collagen I deposition with increasing Ac-ALN and Ca^{2+}/Mg^{2+} concentrations and prolonged time (Fig. S5). In short, the CMS hydrogels facilitated in-situ bone regeneration effectively, and CMS hydrogel containing 300 mM Ac-ALN and 300 mM Ca^{2+}/Mg^{2+} achieved a complete repair effect at 12 weeks.

Various activation factors can also be used to promote the osteogenic ability of hydrogels [39]. However, most importantly, for the updated CMS hydrogel, physical crosslinking consisting of the strong chelation of the comonomer Ac-ALN and Ca^{2+}/Mg^{2+} not only triggered BMSC differentiation toward osteogenesis, further promoting the therapeutic effect of in-situ repair of bone defects, but also presents excellent properties for bone regeneration, compared to HGM hydrogel, because the addition of new physical crosslinking did not damage its original structure. In this study, after being successfully structured with two kinds of physical crosslinking, CMS hydrogel preserved good cytocompatibility with

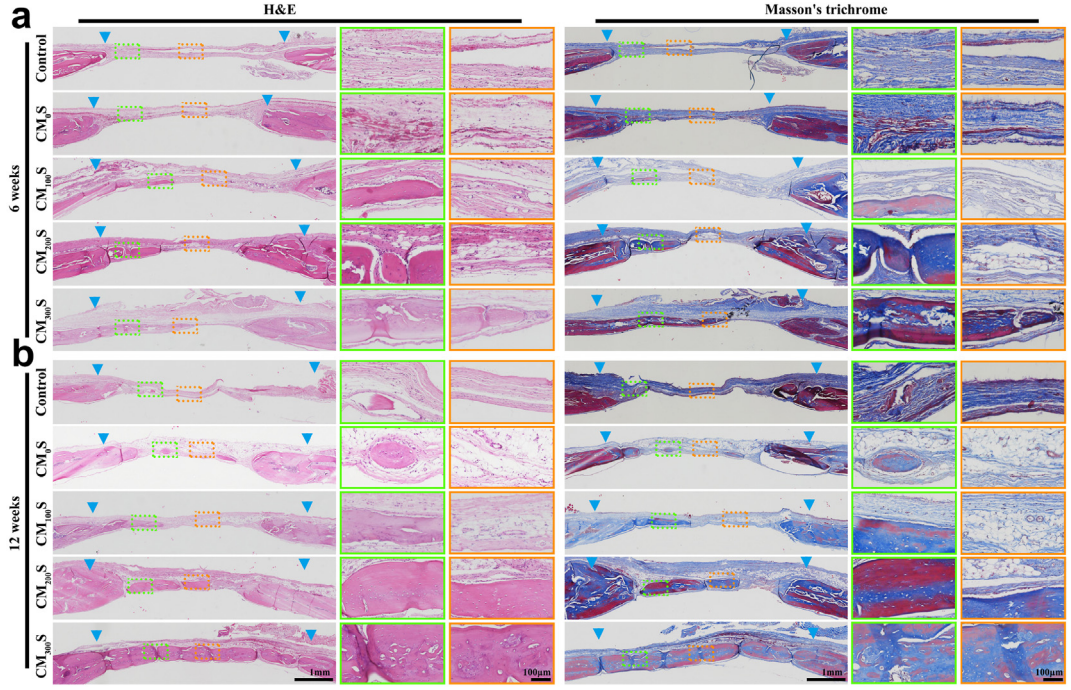

Fig. 7. Histological evaluation of bone regeneration with the different CMS hydrogels at 6 and 12 weeks. (a) H&E and Masson's trichrome staining at 6 weeks; (b) H&E and Masson's trichrome staining at 12 weeks. Orange rectangles indicate repaired tissue in the central defect. Green rectangles indicate repaired tissue in the marginal defect.

BMSCs, like HGM hydrogel, and possessed appropriate drug release properties as well. Furthermore, both the results from *in vitro* osteogenic differentiation and *in-situ* bone regeneration in a cranial defect model showed that the osteogenic effect was enhanced with increasing Ac-ALN and Ca^{2+}/Mg^{2+} concentrations. Therefore, the combination of Ac-ALN and Ca^{2+}/Mg^{2+} represents a favorable choice to fabricate CMS hydrogel for utilization in BTE.

Admittedly, the present study has a few limitations: 1) Despite CMS hydrogel's improved mechanical strength compared to HGM hydrogel, the mechanical properties of CMS hydrogel still have much room for improvement to peruse the application for bearing large-scale bone reconstruction. 2) In this study we chose the rat as the animal model and only performed *in vivo* experiments for a maximum of 12 weeks; hence, studies with a large animal model with a long-term follow-up are warranted to confirm its clinical potential in the future.

4. Conclusion

Herein, using the previously developed HGM hydrogel as the basis, the present study demonstrated an updated supramolecular hydrogel, namely CMS hydrogel, to further fulfill the multifold requirements of applications in BTE. The CMS hydrogel was prepared by adding a new physical crosslinking consisting of the strong chelation of the comonomer Ac-ALN and Ca^{2+}/Mg^{2+} to the HGM hydrogel; this secondary physical crosslinking of Ac-ALN and Ca^{2+}/Mg^{2+} distinctly improved the mechanical properties of CMS hydrogel. Meanwhile, the addition of Ac-ALN and Ca^{2+}/Mg^{2+} physical crosslinking not only did not damage the host-guest interaction structure, but also imparted superior properties such as injectability, self-healing, and excellent cytocompatibility to the CMS hydrogel. Furthermore, the incorporation of Ac-ALN and Ca^{2+} and Mg^{2+} increased CMS hydrogel's efficiency for both stem cell osteogenic differentiation and *in situ* bone regeneration compared to HGM hydrogel. Collectively, the current results indicated that the CMS hydrogel was an appropriate hydrogel for BTE.

Credit author statement

Tao Yu and Yunping Hu, scaffold fabrication, cell cultivation, *in vivo* experiment conduct and amend the work; Wenbao He, data curation, original draft preparation; Yong Xu and Anqi Zhan, data analysis; Kai Chen and Mingxiang Liu, writing-reviewing and editing; Xiufeng Xiao and Xiangyang Xu, conceived the overall technical procedure; Qian Feng, grant supporting; Liangfu Jiang, amend the work.

Declaration of competing interest

The authors declare that they have no known competing financial interests or personal relationships that could have appeared to influence the work reported in this paper.

Data availability

Data will be made available on request.

Acknowledgements

This work is sponsored by Shanghai Pujiang Program (22PJ1409900), National Natural Science Foundation of China (31900963), Fujian Provincial Health and Education Project for Tackling the Key Research (12019-WJ-22), Fuzhou Science and Techonology Project (2020-PT-138), Fundamental Research Funds for the Central Universities (2021CDJQY-017), Zhejiang Provincial Natural Science Foundation (LY20H060005), Shanghai Key Laboratory of Peripheral Nerve and Microsurgery (20DZ2270200), and Medical Health Science and Technology Project of Zhejiang Provincial Health Commission (2020KY649).

Appendix A. Supplementary data

Supplementary data to this article can be found online at https://doi.org/10.1016/j.mtbio.2023.100558.

References

[1] Y. Li, X. Xun, Y. Xu, A. Zhan, E. Gao, F. Yu, Y. Wang, H. Luo, C. Yang, Hierarchical Porous Bacterial Cellulose Scaffolds with Natural Biomimetic Nanofibrous Structure and a Cartilage Tissue-specific Microenvironment for Cartilage Regeneration and Repair, Carbohydr Polym, 2022, 118790, https://doi.org/10.1016/j.carbpol.2021.118790.

[2] Y. Liu, Z. Zhu, X. Pei, X. Zhang, X. Cheng, S. Hu, X. Gao, J. Wang, J. Chen, Q. Wan, ZIF-8-Modified multifunctional bone-adhesive hydrogels promoting angiogenesis and osteogenesis for bone regeneration, ACS Appl. Mater. Interfaces 33 (2020) 36978–36995, https://doi.org/10.1021/acsami.0c12090.

[3] A. Hofmann, S. Gorbulev, T. Guehring, A.P. Schulz, R. Schupfner, M. Raschke, S. Huber-Wagner, P.M. Rommens, Autologous iliac bone graft compared with biphasic hydroxyapatite and calcium sulfate cement for the treatment of bone defects in tibial plateau fractures: a prospective, randomized, open-label, multicenter study, the journal of bone and joint surgery, Americana 3 (2020) 179–193, https://doi.org/10.2106/jbjs.19.00680.

[4] J. Qi, Z. Zheng, L. Hu, H. Wang, B. Tang, L. Lin, Development and characterization of cannabidiol-loaded alginate copper hydrogel for repairing open bone defects in vitro, Colloids Surf. B Biointerfaces (2022), 112339, https://doi.org/10.1016/j.colsurfb.2022.112339.

[5] A. Wubneh, E.K. Tsekoura, C. Ayranci, H. Uludağ, Current state of fabrication technologies and materials for bone tissue engineering, Acta Biomater. (2018) 1–30, https://doi.org/10.1016/j.actbio.2018.09.031.

[6] A. Bharadwaz, A.C. Jayasuriya, Recent Trends in the Application of Widely Used Natural and Synthetic Polymer Nanocomposites in Bone Tissue Regeneration, Materials Science & Engineering. C, Materials for Biological Applications, 2020, 110698, https://doi.org/10.1016/j.msec.2020.110698.

[7] S. Saravanan, S. Vimalraj, P. Thanikaivelan, S. Banudevi, G. Manivasagam, A review on injectable chitosan/beta glycerophosphate hydrogels for bone tissue regeneration, Int. J. Biol. Macromol. (2019) 38–54, https://doi.org/10.1016/j.ijbiomac.2018.10.014.

[8] E. Muscolino, A.B. Di Stefano, M. Trapani, M.A. Sabatino, D. Giacomazza, F. Moschella, A. Cordova, F. Toia, C. Dispenza, Injectable xyloglucan hydrogels incorporating spheroids of adipose stem cells for bone and cartilage regeneration, Mater Sci Eng C Mater Biol Appl (2021), 112545, https://doi.org/10.1016/j.msec.2021.112545.

[9] X. Bai, M. Gao, S. Syed, J. Zhuang, X. Xu, X.Q. Zhang, Bioactive hydrogels for bone regeneration, Bioact. Mater. 4 (2018) 401–417, https://doi.org/10.1016/j.bioactmat.2018.05.006.

[10] Q. Feng, K. Wei, S. Lin, Z. Xu, Y. Sun, P. Shi, G. Li, L. Bian, Mechanically Resilient, Injectable, and Bioadhesive Supramolecular Gelatin Hydrogels Crosslinked by Weak Host-Guest Interactions Assist Cell Infiltration and in Situ Tissue Regeneration, Biomaterials, 2016, pp. 217–228, https://doi.org/10.1016/j.biomaterials.2016.05.043.

[11] C.S. Bae, S.H. Kim, T. Ahn, Y. Kim, S.E. Kim, S.S. Kang, J.S. Kwon, K.M. Kim, S.G. Kim, D. Oh, Basel, Switzerland, Multiple Porous Synthetic Bone Graft Comprising EngineeredMicro-Channel for Drug Carrier and Bone Regeneration, Materials, vol. 18, 2021, https://doi.org/10.3390/ma14185320.

[12] S.K. Boda, H. Wang, J.V. John, R.A. Reinhardt, J. Xie, Dual delivery of alendronate and E7-BMP-2 peptide via calcium chelation to mineralized nanofiber fragments for alveolar bone regeneration, ACS Biomater. Sci. Eng. 4 (2020) 2368–2375, https://doi.org/10.1021/acsbiomaterials.0c00145.

[13] W. Shi, X. Zhang, L. Bian, Y. Dai, Z. Wang, Y. Zhou, S. Yu, Z. Zhang, P. Zhao, H. Tang, et al., Alendronate crosslinked chitosan/polycaprolactone scaffold for bone defects repairing, Int. J. Biol. Macromol. (2022) 441–456, https://doi.org/10.1016/j.ijbiomac.2022.02.007.

[14] M. Asgari, R. Gazor, M.A. Abdollahifar, F. Fadaei Fathabady, F. Zare, M. Norouzian, A. Amini, A. Khosravipour, P. Kiani, R.B. Atashgah, et al., Combined therapy of adipose-derived stem cells and photobiomodulation on accelerated bone healing of a critical size defect in an osteoporotic rat model, Biochem. Biophys. Res. Commun. 1 (2020) 173–180, https://doi.org/10.1016/j.bbrc.2020.06.023.

[15] B.L. Pan, Z.W. Tong, S.D. Li, L. Wu, J.L. Liao, Y.X. Yang, H.H. Li, Y.J. Dai, J.E. Li, L. Pan, Decreased microRNA-182-5p helps alendronate promote osteoblast proliferation and differentiation in osteoporosis via the Rap1/MAPK pathway, Biosci. Rep. (2018) 6, https://doi.org/10.1042/bsr20180696.

[16] S. Datta, A.P. Rameshbabu, K. Bankoti, S. Jana, S. Roy, R. Sen, S. Dhara, Microsphere embedded hydrogel construct - binary delivery of alendronate and BMP-2 for superior bone regeneration, J. Mater. Chem. B. 34 (2021) 6856–6869, https://doi.org/10.1039/d1tb00255d.

[17] D. Li, J. Zhou, M. Zhang, Y. Ma, Y. Yang, X. Han, X. Wang, Long-term delivery of alendronate through an injectable tetra-PEG hydrogel to promote osteoporosis therapy, Biomater. Sci. 11 (2020) 3138–3146, https://doi.org/10.1039/d0bm00376j.

[18] M.J. Sánchez-Fernández, M.R. Immers, R.P. Félix Lanao, F. Yang, J. Bender, J. Mecinović, S.C.G. Leeuwenburgh, J.C.M. van Hest, Alendronate-Functionalized poly(2-oxazoline)s with tunable affinity for calcium cations, Biomacromolecules 8 (2019) 2913–2921, https://doi.org/10.1021/acs.biomac.9b00104.

[19] A. Sahu, Y. Hwang, C. Vilos, J.M. Lim, S. Kim, W.I. Choi, G. Tae, A novel alendronate functionalized nanoprobe for simple colorimetric detection of cancer-associated hypercalcemia, Nanoscale 28 (2018) 13375–13383, https://doi.org/10.1039/c8nr02570c.
[20] G. Kazakova, T. Safronova, D. Golubchikov, O. Shevtsova, J.V. Rau, Resorbable Mg(2+)-containing phosphates for bone tissue repair, Materials 17 (2021), https://doi.org/10.3390/ma14174857.
[21] S. Tharmalingam, C. Wu, D.R. Hampson, The calcium-sensing receptor and integrins modulate cerebellar granule cell precursor differentiation and migration, Dev. Neurobiol. 4 (2016) 375–389, https://doi.org/10.1002/dneu.22321.
[22] R. Cao, A. Zhan, Z. Ci, C. Wang, Y. She, Y. Xu, K. Xiao, H. Xia, L. Shen, D. Meng, et al., A biomimetic biphasic scaffold consisting of decellularized cartilage and decalcified bone matrixes for osteochondral defect repair, Front. Cell Dev. Biol. (2021), 639006, https://doi.org/10.3389/fcell.2021.639006.
[23] Z.T. Bao, Z.P. Gu, J.B. Xu, M. Zhao, G.T. Liu, J. Wu, Acid-responsive composite hydrogel platform with space-controllable stiffness and calcium supply for enhanced bone regeneration, Chem. Eng. J. (2020), https://doi.org/10.1016/j.cej.2020.125353.
[24] W. Jiang, F.S. Hou, Y. Gu, Q. Saiding, P.P. Bao, J.C. Tang, L. Wu, C.M. Chen, C.L. Shen, C.L. Pereira, et al., Local bone metabolism balance regulation via double-adhesive hydrogel for fixing orthopedic implants, Bioact. Mater. (2022) 169–184, https://doi.org/10.1016/j.bioactmat.2021.10.017.
[25] K.Y. Zhang, S.E. Lin, Q. Feng, C.Q. Dong, Y.H. Yang, G. Li, L.M. Bian, Nanocomposite hydrogels stabilized by self-assembled multivalent bisphosphonate-magnesium nanoparticles mediate sustained release of magnesium ion and promote in-situ bone regeneration, Acta Biomater. (2017) 389–400, https://doi.org/10.1016/j.actbio.2017.09.039.
[26] Y.A. Qing, H. Wang, Y. Lou, X. Fang, S.H. Li, X.Y. Wang, X. Gao, Y.G. Qin, Chemotactic ion-releasing hydrogel for synergistic antibacterial and bone regeneration, Mater. Today Chem. (2022) https://doi.org/ARTN 100894 10.1016/j.mtchem.2022.100894.
[27] X. Liu, Z.J. Ren, F.F. Liu, L. Zhao, Q.J. Ling, H.B. Gu, Multifunctional self-healing dual network hydrogels constructed via host-guest interaction and dynamic covalent bond as wearable strain sensors for monitoring human and organ motions, Acs Appl. Mater Inter. 12 (2021) 14625–14635, https://doi.org/10.1021/acsami.1c03213.
[28] J.C. Liu, S. Bao, Q.J. Ling, X. Fan, H.B. Gu, Ultra-fast preparation of multifunctional conductive hydrogels with high mechanical strength, self-healing and self-adhesive properties based on Tara Tannin-Fe3+ dynamic redox system for strain sensors applications, Polymer (2022) https://doi.org/ARTN 12451310.1016/j.polymer.2021.124513.
[29] Z.J. Ren, T. Ke, Q.J. Ling, L. Zhao, H.B. Gu, Rapid self-healing and self-adhesive chitosan-based hydrogels by host-guest interaction and dynamic covalent bond as flexible sensor, Carbohydr. Polym. (2021) https://doi.org/ARTN_11853310.1016/j.carbpol.2021.118533.
[30] X. Fan, L. Zhao, Q.J. Ling, H.B. Gu, Tough, self-adhesive, antibacterial, and recyclable supramolecular double network flexible hydrogel sensor based on PVA/Chitosan/Cyclodextrin, Ind. Eng. Chem. Res. 10 (2022) 3620–3635, https://doi.org/10.1021/acs.iecr.1c04997.
[31] F.F. Liu, X. Liu, H.B. Gu, Multi-network poly(beta-cyclodextrin)/PVA/Gelatin/Carbon nanotubes composite hydrogels constructed by multiple dynamic crosslinking as flexible electronic devices, Macromol. Mater. Eng. 3 (2022) https://doi.org/ARTN 2100724_10.1002/mame.202100724.
[32] Q.J. Ling, F.C. Zhen, D. Astruc, H.B. Gu, ROMP synthesis of side-chain ferrocene-containing polyelectrolyte and its redox-responsive hydrogels showing dramatically improved swelling with beta-cyclodextrin, Macromol. Rapid Commun. 11 (2021) https://doi.org/ARTN 2100049 10.1002/marc.202100049.
[33] X. Fan, J.H. Geng, Y.L. Wang, H.B. Gu, PVA/gelatin/beta-CD-based rapid self-healing supramolecular dual-network conductive hydrogel as bidirectional strain sensor, Polymer (2022) https://doi.org/ARTN 124769 10.1016/j.polymer.2022.124769.
[34] X. Zhai, C. Ruan, J. Shen, C. Zheng, X. Zhao, H. Pan, W.W. Lu, Clay-based nanocomposite hydrogel with attractive mechanical properties and sustained bioactive ion release for bone defect repair, J. Mater. Chem. B 10 (2021) 2394–2406, https://doi.org/10.1039/d1tb00184a From NLM.
[35] M. Leidi, F. Dellera, M. Mariotti, J.A. Maier, High magnesium inhibits human osteoblast differentiation in vitro, Magnes. Res. 1 (2011) 1–6, https://doi.org/10.1684/mrh.2011.0271 From NLM.
[36] D. Zhang, N. Ni, Y. Su, H. Miao, Z. Tang, Y. Ji, Y. Wang, H. Gao, Y. Ju, N. Sun, et al., Targeting local osteogenic and ancillary cells by mechanobiologically optimized magnesium scaffolds for orbital bone reconstruction in canines, ACS Appl. Mater. Interfaces 25 (2020) 27889–27904, https://doi.org/10.1021/acsami.0c00553 From NLM.
[37] M.N. George, X. Liu, A.L. Miller 2nd, H. Xu, L. Lu, Phosphate functionalization and enzymatic calcium mineralization synergistically enhance oligo[poly(ethylene glycol) fumarate] hydrogel osteoconductivity for bone tissue engineering, J. Biomed. Mater. Res. Part A. 3 (2020) 515–527, https://doi.org/10.1002/jbm.a.36832 From NLM.
[38] P. Gao, B. Fan, X.M. Yu, W.W. Liu, J. Wu, L. Shi, D. Yang, L.L. Tan, P. Wan, Y.L. Hao, et al., Biofunctional magnesium coated Ti6Al4V scaffold enhances osteogenesis and angiogenesis in vitro and in vivo for orthopedic application, Bioact. Mater. 3 (2020) 680–693, https://doi.org/10.1016/j.bioactmat.2020.04.019.
[39] Y. Wu, X. Zhang, Q. Zhao, B. Tan, X. Chen, J. Liao, Role of hydrogels in bone tissue engineering: how properties shape regeneration, J. Biomed. Nanotechnol. 12 (2020) 1667–1686, https://doi.org/10.1166/jbn.2020.2997 From NLM.